Available free online at www.medjchem.com

Mediterranean Journal of Chemistry

Mediterranean Journal of Chemistry **2025**, 15(1), 44-55

Removal of methyl orange in Aqueous Media using two clays from Côte d'Ivoire

Koné Yetchiè Tchonrontcha [1], Abollé Abollé [1], Kambiré Ollo [2,*], Koffi Konan Sylvestre[3], Kouadio Kouakou Etienne [3] and Kimou Kouakou Jocelin [3]

[1] Laboratoire de Thermodynamique et Physico-Chimie du Milieu, UFR Sciences Fondamentales et Appliquées, Université Nangui Abrogoua, 02 BP 801 Abidjan 02, Côte d'Ivoire

[2] UFR Sciences et Technologies, Université de Man, BP 20 Man, Côte d'Ivoire

[3] Laboratoire de constitution et réaction de la matière, UFR SSMT, Université Félix Houphouët-Boigny de Cocody, Abidjan, 22 BP 582 Abidjan 22, Côte d'Ivoire

Abstract: This work used Boundiali and Man clays to eliminate methyl orange in an aqueous medium. These clays were activated with hydrochloric acid and then characterized by scanning electron microscopy, X-ray diffractogram, Brunauer–Emmett–Teller (BET) method, and zero charge pH. Methyl orange concentration was monitored during adsorption using a UV-visible spectrophotometer. Characterization showed that the clays have many micropores, mesopores, and few macropores. The specific surface areas of these clays are equal to 39,084 $m^2\ g^{-1}$ and 39,722 $m^2\ g^{-1}$ for Boundiali and Man clays, respectively. These clays are composed of kaolinite, illite, and quartz. They have non-uniform morphologies and display irregularly shaped flaky particles of different sizes. The surface pH of Boundiali clay is neutral, while Man clay's is essential. Adsorption of methyl orange on these clays conforms to pseudo 2nd order kinetics with 60 minutes as the equilibrium time. Adsorption is favorable in acidic media and spontaneous at room temperature with both types of clay. The Boundiali clay has an adsorption capacity of 40.486 mg $g^{-1,}$ and the Man clay has an adsorption capacity of 38.610 mg g^{-1}.

Keywords: Activated clay, methyl orange, adsorption, kinetics, isotherm.

1. Introduction

Increasing levels of industrial pollutants discharged into the environment as waste seriously threaten human health, life, resources, and ecological systems [1-3]. Among these pollutants are dyes from the textile industry, which contribute to environmental pollution [4, 5]. Most dyes used in the textile industry are not biodegradable and tend to cause various disorders and diseases in living organisms [6, 7]. Consequently, effluents containing dyes from the textile industry must treated before being discharged into water.

Several treatment methods contribute to eliminating industrial dyes, such as advanced oxidation processes, electrochemical methods, and solid adsorption methods [8-12]. Regarding adsorption, activated carbon treatment has been widely used [10, 13, 14]. However, activated carbon is expensive compared with clay, which is abundant and almost free in our country (Côte d'Ivoire). In addition, clays have a high adsorption capacity for trace metals and organic compounds in aqueous media. This is due to their large specific surface areas [15, 16]. In addition, clay is an abundant material throughout Côte d'Ivoire [17].

According to the literature, clays from Côte d'Ivoire have given excellent results in the adsorption of trace metals and certain organic compounds [15-17]. This is the context of this study. Our objective is to treat wastewater containing methyl orange with local clays. This is why we propose treating water polluted by methyl orange (MO) using Boundiali and Man clays in this work. The clays from these two regions were chosen to compare two clays from different climates. Boundiali is a town located in the north of Côte d'Ivoire in a grassy savannah where rainfall is low. The city of Man is located in a forested area with abundant rainfall in the west of Côte d'Ivoire. Boundiali and Man clays will be activated by hydrochloric acid to increase their specific surface area or total pore volume [18-20]. They will then be characterized by scanning electron microscopy (SEM), X-ray diffraction (XRD), the Brunauer, Emmett, and Teller (BET) method, and zero charge pH (pHpzc). The adsorption of methyl orange was investigated by studying adsorption kinetics, the Influence of pH on adsorption, and the application of the Freundlich and Langmuir Isotherm models.

**Corresponding author: Kambiré Ollo*
Email address: kambireollo@yahoo.fr
DOI: http://dx.doi.org/10.13171/mjc02501081810ollo

Received September 30, 2024
Accepted Novembre 5, 2024
Published January 8, 2025

2. Materials and methods

2.1. Clay preparation

The clay was prepared in four stages: crushing and sieving, dispersion in water, phase separation, and acid etching.

Crushing and sieving consisted of grinding the clay in a porcelain mortar and sieving it with a series of sieves ranging in size from 250 µm, 160 µm, and 100 µm to obtain a fine powder with a size of less than 100 µm. Dispersion is achieved by weighing 12 g of clay and introducing it into 360 mL of distilled water. The mixture is left to stir for 24 hours. The mixture is filtered through a 40 µm diameter filter paper to separate the solid and liquid phases. It was then dried in an oven at 60°C for 24 hours. Acid etching consists of weighing 5 g of the clay obtained after drying and introducing it into 100 mL of a 1 M hydrochloric acid solution. The mixture obtained is left to stir for 24 hours and then filtered. After filtration, it is dried in an oven for 24 hours at 60°C and stored in airtight jars.

2.2. MO solution preparation

A concentrated solution of MO with a concentration (100 mg L^{-1}) was prepared from commercial MO. Successive dilutions of the concentrated solution were obtained for the solutions used in this study. The pH of these solutions was adjusted with hydrochloric acid and sodium hydroxide. The properties of methyl orange are shown in Table 1.

Table 1. MO characteristics

Name	Methyl orange (C.I. 13025) PA-ACS
Family	Acid dye
Formula	$C_{14}H_{14}N_4NaO_3S$
Structure	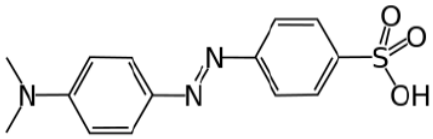
Molar mass	327.336 g.mol^{-1}
λ_{max}	465 nm
Solubility	5.2 g L^{-1} in water at 20°C; 1.0 g L^{-1} in ethanol at 20°C

2.3 Quantity of MO adsorbed

The amount of MO adsorbed was calculated using the following relation [16]:

$$q_t = \frac{C_0 - C_t}{m} \times V \quad (1)$$

Where q_t is the quantity of dye adsorbed per unit mass of adsorbent in mg/g, C_0 is MO concentration at time t = 0 in mg/L, C_t is the residual concentration of MO at time t in mg L^{-1}, V is the volume of the reaction mixture in L and m is the mass of adsorbent in g.

2.4. Determination of adsorption rate

The adsorption rate of MO on clays is obtained according to the following formula [16]:

$$\text{Taux d'adsorption } (\%) = \frac{(C_0 - C_t)}{C_0} \times 100 \quad (2)$$

Where C_0 is the concentration of MO at time t = 0 in mg L^{-1}, and C_t is the residual concentration of MO at time t in mg L^{-1}.

2.5. Adsorption kinetic model

Three kinetic models were applied to MO adsorption onto clays. These were the Pseudo 1st order, Pseudo 2nd order, and intraparticle diffusion kinetic models. Equations 3, 4, and 5 were used to apply the Pseudo 1st order, Pseudo 2nd order, and intraparticle diffusion kinetic models, respectively [21, 22].

$$ln(q_e - q_t) = ln(q_e) - k_1 t \quad (3)$$

$$\frac{t}{q_t} = \frac{1}{k_2 q_e^2} + \frac{1}{q_e} t \quad (4)$$

$$q_t = k_i t^{1/2} + C \quad (5)$$

Where q_t and q_e the quantities of dye adsorbed respectively at instants t, and at equilibrium in (mg g^{-1}), t is the contact time in min, k_1, k_2, and k_i are the rate constants for adsorption of the dye onto the adsorbent.

2.6. Isotherm model

Freundlich and Langmuir's adsorption isotherm models were applied to the adsorption of methyl orange on clays using equations 6 and 7.
Freundlich equation can written as [21, 23]

$$q_e = K_F C_e^{1/n} \quad (6)$$

Langmuir equation can written as [21, 23]

$$q_e = \frac{q_m b C_e}{1 + b C_e} \quad (7)$$

Wherev C_e is the equilibrium concentration of the dye in the residual solution in mg L^{-1}, q_e is the quantity of dye adsorbed per unit mass of adsorbent at equilibrium in mg g^{-1}, q_m is the quantity of dye adsorbed per gram of adsorbent in mg g^{-1}, K_F, and n are the Freundlich constants and b is the Langmuir thermodynamic constant related to the free energy of adsorption.

3. Results and Discussion

3.1. Characterisation of clays

3.1.1. Characterisation by scanning electron microscopy (SEM)

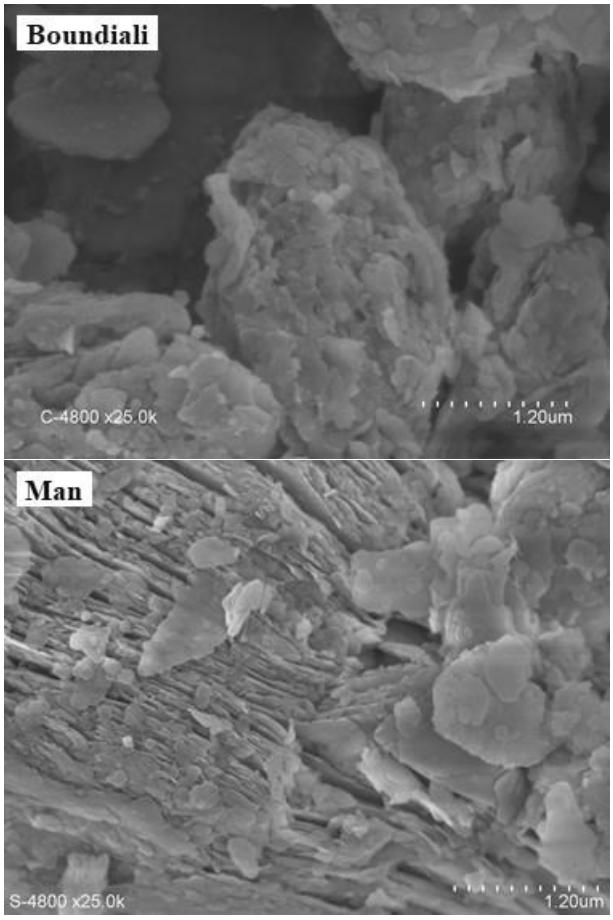

Fig. 1. SEM images of clays

Fig.1 shows SEM images of the outer surface of the activated clays of Boundiali and Man. These images show that Boundiali clay is divided into several blocks on which a disordered assembly of sheets can observed. SEM image of Man shows that this material is made up of microscopically planar sheets that are detached and arranged parallel to one another. SEM images of these clays show adsorption capacities; they have non-uniform morphologies and display irregularly shaped laminated particles of different sizes. This difference in size may be affected by the association of much larger aggregates with the natural clay particles before their activation. SEM images of these two clays show different structures. This explains why the clays differ according to their structure and the region from which they were extracted.

3.1.2. Characterisation by X-ray diffractogram

Fig. 2 shows the X-ray Diffraction peaks of the two clays. XRD spectra of the activated clays from Boundiali show kaolinite peaks at 2θ: 12.54°, 21.05°, 38.47°, 42.96°;55.40° and 60.12°. Illite peaks at 25.21°; 35.07° and quartz peaks at 2θ corresponding to 26.86°; 50.32° and 68.37°. As for Man clay: 2θ angles equal to 12.37°; 20.06°; 20.98°; 38.67°; 46.06° are characteristic of kaolinite. Those 8.97°, 25.04°, and 55.07° represent the angles at which illite appears. The angles 26.79°; 50.22°; 60.06° and 68° belong to quartz peaks.

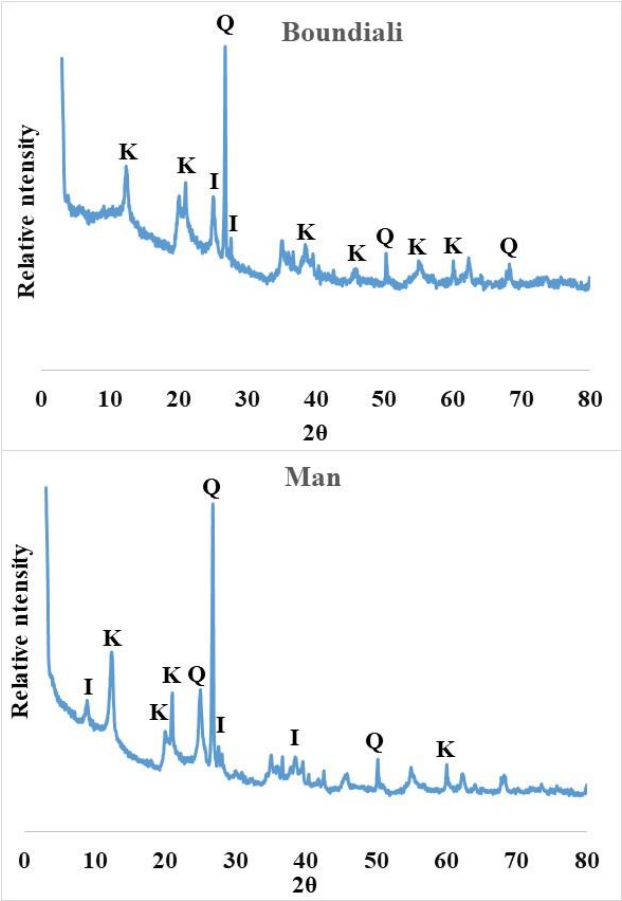

Fig. 2. XRD of activated clays (kaolinite (K), illite (I), and quartz (Q)

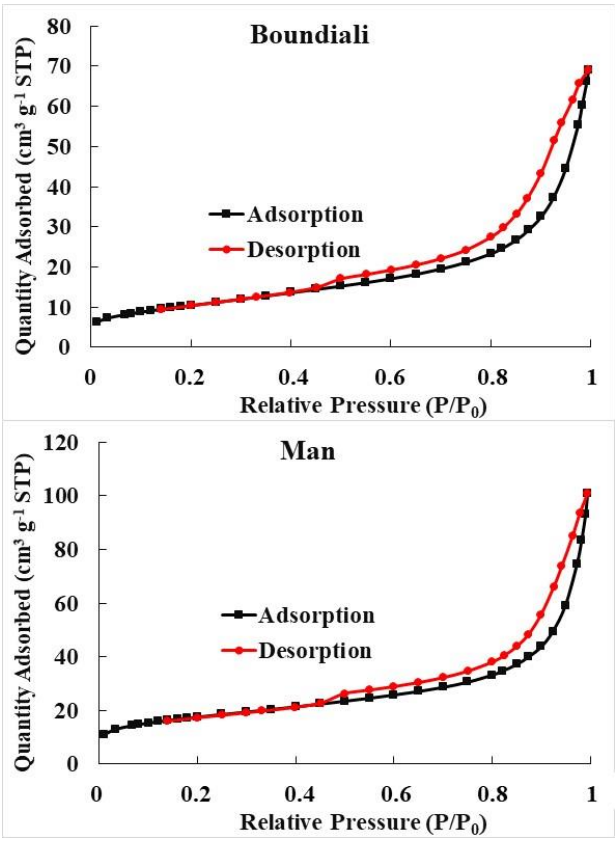

Fig. 3. Adsorption isotherm for N_2 on activated clay from Boundiali and Man

3.1.3. Characterisation by BET

The textural properties, BET, size distribution, and pore volume were determined by the physisorption of N_2 at -195.832°C. The adsorption/desorption isotherms of azote at 77 K are shown in Fig. 3. The quantities of gas adsorbed are shown as a function of the relative pressure P/P_0, where P represents the azote pressure at equilibrium, and P_0 is the saturated vapor pressure of the azote at the temperature considered. Two types of relative pressure appear on each of these figures. The first range, corresponding to a relative pressure of approximately 0 and 0.45, describes the adsorption of a monolayer of gas on the external surfaces and the filling of micropores of openings ranging from 0 to 2 nm. The second zone, with a relative pressure P/P0 between 0.45 and 0.98, describes multilayer adsorption, followed by capillary condensation with desorption, revealing a hysteresis block, that of adsorption for P/P0 greater than or equal to 0.45.

The specific surface area, the pore volume, and the micropores of these clays are determined and shown in Table 2.

Table 2. Textural characteristics of Boundiali and Man clays.

Samples	BET Specific surface area [m^2 g^{-1}]	Micropore volume [cm^3 g^{-1}]	Pore volume [cm^3 g^{-1}]
Boundiali	39,084	0.109	0.139
Man	39,722	0,083	0,106

BET analysis revealed that the clays have large specific surface areas of 39,084 m^2 g^{-1} and 39,722 m^2 g^{-1}, respectively for the Boundiali and Man clays. These results are similar to those found by [15, 16, 24]. These values show that Man clay's specific surface area is higher than the Boundiali clay's. We also observe that the pore volume of Man clay is higher than that of Boundiali, in contrast to the micropore volume.

3.1.4. Zero charge pH (pHpzc)

pHpzc indicates the chemical and electronic properties of the adsorbent's functional groups. The surface of the adsorbent becomes positively charged if pH < pHpzc and negatively charged if pH > pHpzc [24]. The results in Fig. 4 were used to determine the pHpzc of the two types of clay. The values obtained are shown in Table 3. 7.00 and 7.70 were obtained with the Boundiali and Man clays, respectively. These results show that the surface of Boundiali clay is neutral, and Man clay's is slightly basic.

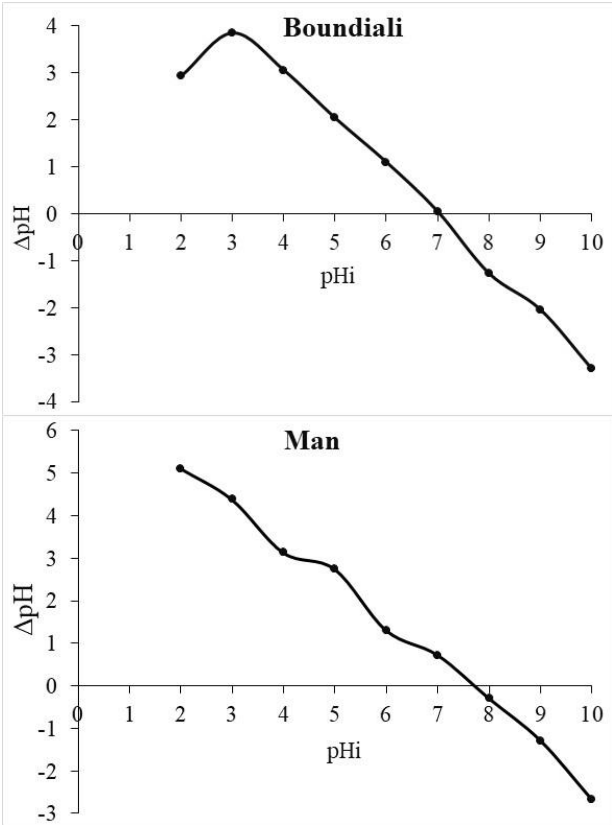

Fig. 4. Zero charge pH of clays

Table 3. Zero charge pH values.

Clay	Boundiali	Man
pH zero charge	7.00	7.70

The functional groups on the clay surface will be protonated by proton H^+ when the pH of the solution studied is lower than pHpzc. The adsorbent becomes an attractor of negatively charged adsorbate. When the study medium pH is higher than pHpzc, the adsorbent becomes a positively charged adsorbate attractor. In this case, the functional groups on the clay surface will be deprotected by the presence of hydroxide ions *(OH^-)* in solution [16, 25].

3.2. Adsorption kinetics of MO

3.2.1. Influence of contact time

The Influence of contact time on MO adsorption clays was studied. The results are shown in Fig. 5. This figure shows a rapid increase in the rate of MO elimination in the first 20 minutes. This data indicates a rapid rise in the quantities adsorbed during the first 20 minutes with each clay type. This rapid adsorption corresponds to MO adsorption on most accessible sites, probably on the sites located on the external surfaces of the clays. After these 20 minutes, slow adsorption was observed, eventually reaching equilibrium at 60 min with both types of clay. This can be attributed to diffusion into less accessible pores such as micropores. The sites become less and less available, resulting in diffusion towards the less accessible sites, slowing down the adsorption rate before reaching equilibrium. Saturation of the accessible sites occurs after 60 min, which corresponds to the equilibrium time for MO adsorption on clays [25, 26].

Fig. 5 shows that MO adsorption rates on these clays at equilibrium are equal to 80% for Boundiali and 61% for Man clay. MO adsorption rate is higher with the Boundiali clay than with Man clay because the zero charge pH of Man clay is neutral, whereas that of Boundiali clay is weakly basic. These results show that Man clay is more suitable for adsorbing an anionic dye such as MO.

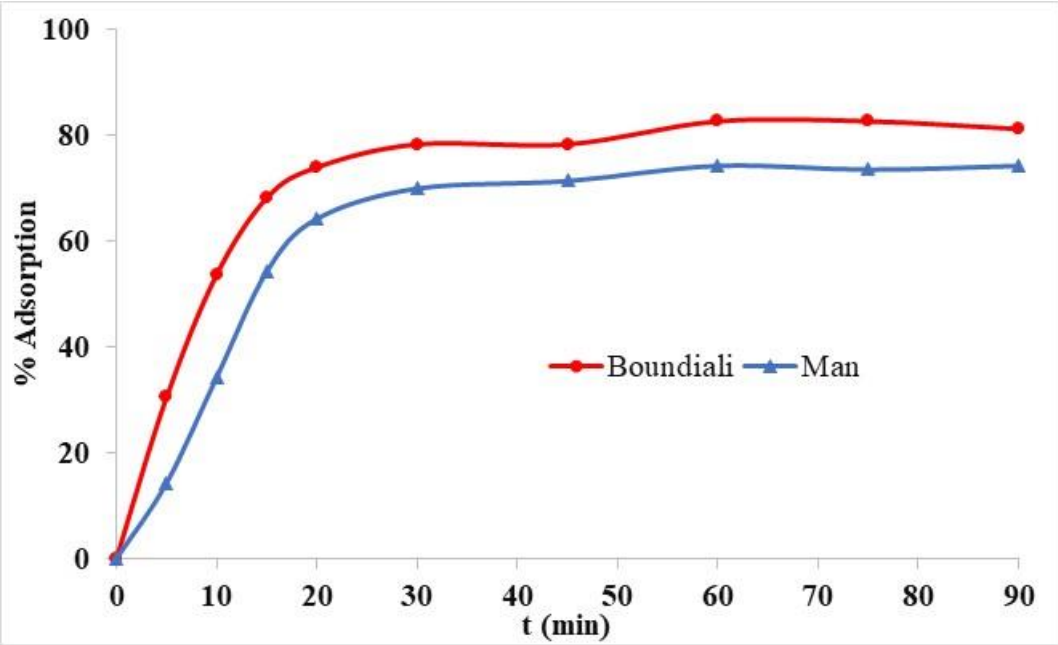

Fig. 5. MO removal efficiency on different types of clay; clay mass = 3 g; MO concentration 10 mg/L

3.2.2 Modelling of adsorption kinetics

Pseudo-first-order, pseudo-second-order, and intraparticle diffusion kinetic models were applied to the MO adsorption on the two clay types. The results obtained are presented in Fig. 6.

The characteristic values of these models are shown in Table 4. This table shows that the coefficients of determination obtained with the pseudo-second-order kinetic model are higher than those obtained with the pseudo-first-order and intraparticle diffusion kinetic models for both types of clay. This shows that pseudo-second-order kinetics are better adapted to the adsorption of MO on these clays. In addition, we note that with the kinetic model of intraparticle diffusion, the curves $q_t = f(t^{1/2})$ are straight lines that do not pass through the origin of the reference frame. We also note that the theoretical values for the maximum quantity of MO adsorbed with the pseudo-first-order model are much lower than those for the pseudo-second-order kinetic model, and those for the pseudo-second-order model are closer to the experimental values. These results confirm that the two clays' pseudo-order kinetic model is the most suitable for our study. This implies that the dye adsorption process on our clays is governed by a bimolecular process

consisting of a collision between an active clay site and a dye molecule [16]. These results are similar to those obtained with the adsorption of methylene blue on Bouaflé clay [15].

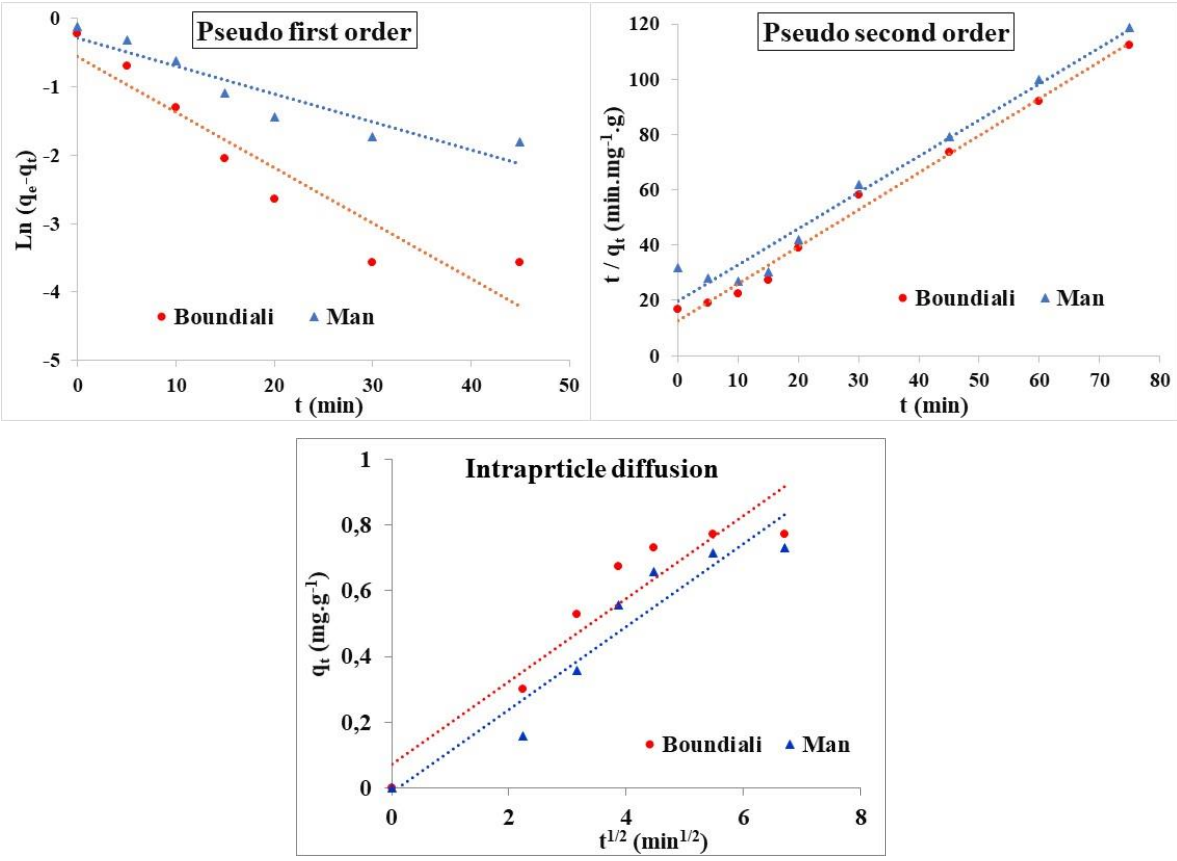

Fig. 6. Application of the pseudo-first-order, pseudo-second-order, and intraparticle diffusion kinetic model to the adsorption of MO on clays

Table 4. Parameters of the MO adsorption kinetics models on the two clay types.

Clay	q_e (mg g^{-1})	Pseudo-first-order			Pseudo -second-order			Intraparticle diffusion	
		k_1 (min^{-1})	R^2	q_{th}	k_2 (g mg^{-1} min^{-1})	R^2	q_{th}	k_i (mg g^{-1} min$^{-1/2}$)	R^2
Boundiali	0.815	0.081	0.886	0.570	0.144	0.991	0.747	0.126	0.894
Man	0.758	0.041	0.868	0.753	0.086	0.969	0.765	0.125	0.912

3.3 Application of Freundlich and Langmuir Isotherm models

The adsorption of several concentrations of methyl orange on Boundiali and Man clays was carried out. The results made it possible to determine the adsorption isotherms for methyl orange on the two types of clay (Fig. 7). It can be seen that the adsorbed quantities of the dye increase with the equilibrium concentration, indicating a high adsorption capacity of the clays for methyl orange. Adsorption of methyl orange, therefore, takes place on a monolayer [27]. Consequently, various mathematical models can be applied to determine the maximum adsorption capacities (q_{max}) and other characteristic parameters. Linearization of the various isotherms using Langmuir and Freundlich models are shown in Fig. 8. Based on the linearization results, the parameters of the adsorption isotherm models are grouped together in Table 5.

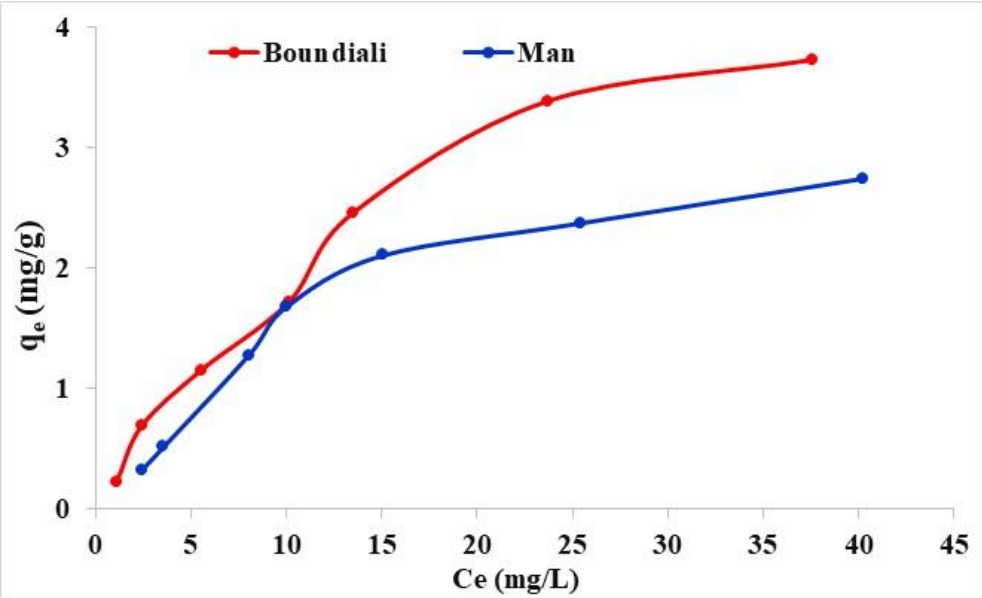

Fig. 7. Adsorption isotherms for methyl orange on the two clays

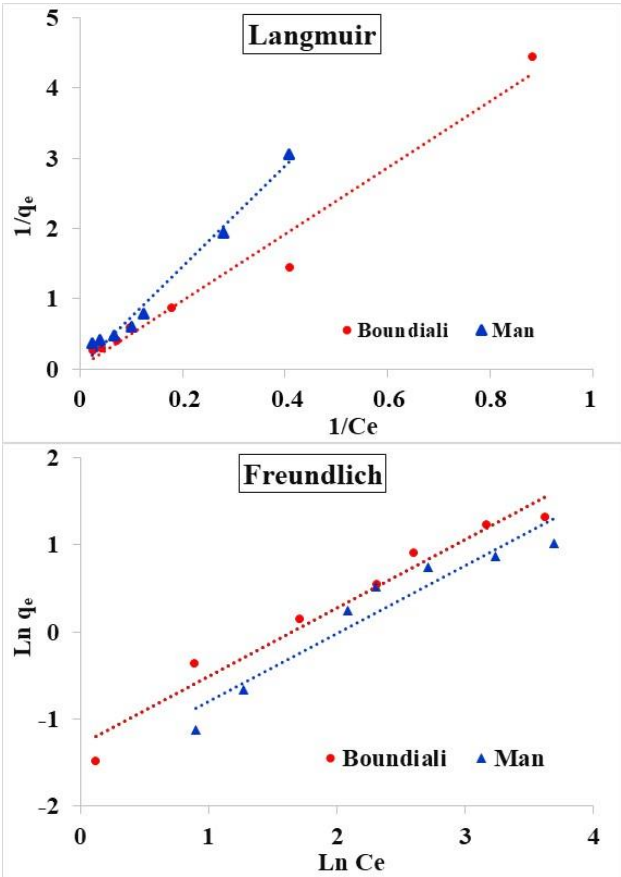

Fig. 8. Representation of the Langmuir and Freundlich models applied to the adsorption of MO on clays.

The coefficients of determination obtained with Boundiali and Man clays are respectively equal to 0.974 and 0.984 for the Langmuir model. The coefficient of determination values of 0.962 and 0.917 were obtained with Boundiali and Man clays by applying the Freundlich model. These values indicate that Boundiali clay's coefficients of determination with Langmuir and Freundlich models are close, thus showing that the two isotherm models are applicable to this clay. However, with Man clay, the value of the coefficient of determination R^2 obtained with Langmuir is higher than that of Freundlich. This indicates that the adsorption of methyl orange on Man clay is better described by the Langmuir model, suggesting chemisorption with the formation of a

monolayer. The adsorption of MO on this clay would, therefore, be localized to sites of the same energy.

The values of the constant "n" obtained with the Freundlich model indicate the degree of non-linearity between the concentration of the solution and the adsorption. Adsorption of the dye onto the clay is linear if $n = 1$. When $n < 1$, dye adsorption is a chemical process. Adsorption is a physical process if $n > 1$ [28]. Table 6 shows that the n value in the Freundlich equation is greater than 1 for the adsorption of MO on both types of clay. These values show that dye adsorption on these two clays is a physical process. The values of n are between 1 and 10. This indicates that there is good adsorption [28, 29]. The data in Table 6 also show that MO adsorption on the different clay types is spontaneous at room temperature. The Langmuir constant "KL" values linked to the interaction force are all positive.

Table 5. Parameters of Langmuir and Freundlich equations for the five clays.

Clay	Freundlich Isotherm			Langmuir Isotherm		
	K_f	R^2	n	K_L	R^2	q_m (mg g^{-1})
Boundiali	0.272	0.962	1.270	0.005	0.974	40.486
Man	0.208	0.917	1.287	0.004	0.984	38.610

These results show that Boundiali clay has an adsorption capacity of 40.486 mg g^{-1}. Man's clay has an adsorption capacity of 38.610 mg g^{-1}. These high adsorption capacities can be explained by their high specific surface area. The maximum quantities of dyes adsorbed by various materials are shown in Table 6. This table shows that our two clays can effectively remove MO in an aqueous solution.

Table 6. Maximum dye adsorption capacity for several types of material.

Materials	**Adsorbed dye**	**q_m (mg g^{-1})**	**Reference**
Bottom Ash	Methyl orange	3.618	30
De-Oiled Soya	Methyl orange	16.664	30
Activated carbon modified by ethylenediaminetetraacetic acid	Rhodamine B	7.11	31
Activated carbon modified by ethylenediaminetetraacetic acid	Methylene blue	7.40	31
Clay modified with cetyltrimethammonium bromide	Methyl orange	15.58	32
Bouaflé clay	Methylene blue	23.256	15
Boundiali clay	Methyl orange	40.486	This study
Man clay	Methyl orange	38.610	This study

3.4. Influence of pH on adsorption

The pH of the medium gives an idea of the state of the surface charge of the adsorbent and the adsorbate. Fig. 9 shows the Influence of pH on MO adsorption on the different types of clay. The stirring time corresponds to the equilibrium of each material during its kinetic study. The adsorption rate is high in acidic media and decreases with increasing pH for all clays. These results for MO adsorption on Boundiali and Man clays are comparable to those found in the literature [16, 33, 34]. The maximum adsorption rate values were obtained at pH 2.3. The values obtained at this pH equal 84.00% and 82.09%, respectively, for Boundiali and Man clays. It should also be noted that the pH values with the lowest MO elimination rates were obtained at a pH equal to 10.1. Boundiali and Man clays achieved adsorption rates of 29.03% and 27.42%, respectively, at this pH.

When the pH is lower than pHpz, the number of positively charged sites in the active clay increases, thus favoring MO adsorption, an anionic dye, via electrostatic attraction [35]. A decrease in the absorption rate observed in an essential environment (pH > pHpzc) is thought to be due to excess hydroxide ions, which compete with the dye, MO molecules. The increase in pH leads to increased hydroxyl ions, which bind to the clay surface. As a result, the adsorption of MO becomes unfavorable due to electrostatic repulsion.

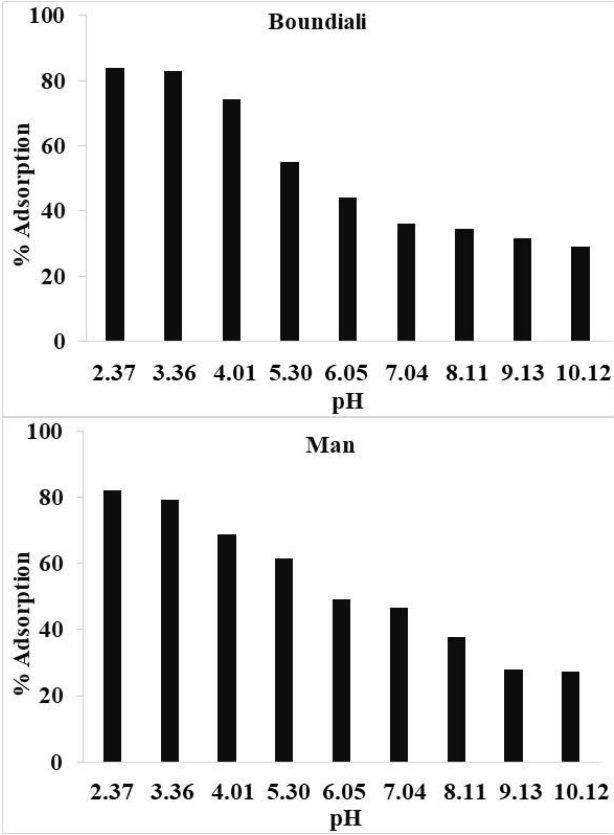

Fig. 9. Effect of pH on the adsorption of MO on the two types of clay

4. Conclusion

Clays from Boundiali and Man were characterized and used to remove methyl orange (MO) in an aqueous solution. Characterization by BET showed that the clays have many micropores, mesopores, and few macropores. Determination of the specific surface areas gave 39,084 m^2 g^{-1} and 39,722 m^2 g^{-1} for the activated clays from Boundiali and Man, respectively. X-ray diffraction showed that these clays comprise kaolinite, illite, and quartz. SEM analysis of these clays showed that they have non-uniform morphologies and display irregularly shaped flaky particles of different sizes. Zero charge pH showed that the surface pH of Boundiali clay is neutral, and Man clay's is slightly basic. The kinetic study of MO adsorption on these clays showed that adsorption conforms to pseudo-2nd-order kinetics with 60 minutes as the equilibrium time. MO adsorption on these clays is favorable in an acid medium. Langmuir and Freundlich's adsorption isotherm models were applied to the adsorption of MO on Boundiali clay. However, only Langmuir adsorption isotherm better describes MO adsorption on Man clay. Adsorption of MO on these clays is spontaneous at room temperature. Boundiali clay has an adsorption capacity of 40.486 mg $g^{-1,}$ and Man clay has an adsorption capacity of 38.610 mg g^{-1}.

Conflict of interest

There is no conflict of interest between the co-authors of this work.

References

1. H. B. Slama, A. C. Bouket, Z. Pourhassan, F. N. Alenezi, A. Silini, H. Cherif-Silini, T. Oszako, L. Luptakova, P. Golińska, L. Belbahri, Diversity of Synthetic Dyes from Textile Industries, Discharge Impacts and Treatment Methods, Appl. Sci., **2021**, 11(14), 6255.
2. D. Li, Z. Gao, B. Zhang, W. Ma, B. Tang, S. Zhang, Excellent fixation of low-water-soluble reactive dyes containing vinylsulfone group for nylon dyeing, Dyes and Pigments, **2024**, 222, 111887.
3. Y. Wang, T. Zhao, X. Bi, C. lv, Synthesis of novel carbene dyes and investigation of their dyeing properties and reaction mechanism for various fabrics. Dyes and Pigments, **2024** 221, 111784.
4. X. Liu, J. Wang, Decolorization and degradation of various dyes and dye-containing wastewater treatment by electron beam radiation technology: An overview. Chemosphere, **2024**, 351, 141255.
5. S. Zinatloo-Ajabshir, S. Rakhshani, Z. Mehrabadi, M. Farsadrooh, M. Feizi-Dehnayebi, S. Rakhshani, M. Dušek, V. Eigner, S. Rtimi, T. M. Aminabhavi, Novel rod-like [Cu(phen)2(OAc)]·PF6 complex for high-performance visible-light-driven photocatalytic degradation of hazardous organic dyes: DFT approach, Hirshfeld and fingerprint plot analysis.

Journal of Environmental Management, **2024**, 350, 119545.
6. K. Moro, A. S. Ello, K. R. Koffi, N. S. Eroi, Mixed Maghemite/Hematite Iron Oxide Nanoparticles Synthesis for Lead and Arsenic Removal from Aqueous Solution, Journal of Nanomaterials, **2023**, Article ID 8216889, 8.
7. A. M. Gutierrez, T. D. Dziubla, J. Z. Hilt, Recent advances on iron oxide magnetic nanoparticles as sorbents of organic pollutants in water and wastewater treatment, Reviews on Environmental Health, **2017**, 32, (1-2), 111-117.
8. O. Kambiré, L. A. G. Pohan, S. P. Sadia, K. E. Kouadio, L. Ouattara, Voltammetric study of formic acid oxidation via active chlorine on IrO_2/Ti and RuO_2/Ti electrodes. Mediterranean Journal of Chemistry, **2020**, 10(8), 799-808.
9. L. A. G. Pohan, O. Kambiré, M. Nasir, L. Ouattara, Photocatalytic and Antimicrobial Properties of [$AgTiO_2$]:[Clay] Nanocomposite Prepared with Clay Different Ratios, Modern Research in Catalysis, **2020**, 9, 47-61.
10. Y. U. Kouakou, O. Kambiré, N. S. Eroi, Y. T. Koné, A. Trokourey, Kinetic and Thermodynamic Study of the Elimination of Remazol Black on Activated Carbon Based on Ricinodendron heudelotii Shells. Journal of Materials Science and Chemical Engineering, **2023**, 11, 1-20.
11. O. Kambiré, A. Abollé, A. R. Kouakou, A. E. Koffi, K. S. Koffi, K. E. Kouadio, K. J. Kimou, S. Koné, L. Ouattara, Oxidation of rhodamine B using the Fenton process: optimization, kinetics and inorganic ions studies. Journal de la Société Ouest-Africaine de Chimie, **2022**, 051, 45-55.
12. N. L. B. Kouassi, D. Diabate, L. A. G. Pohan, B. D. Ossonon, L. D. Blonde, A. Trokourey, Green Synthesis of Iron Oxide Nanoparticles Using Grapefruit Peel Extract: Application for Removal of Indigo Carmine Dye from Industrial Wastewate. American Journal of Physical Chemistry, **2022**, 11(4), 110-119.
13. A. Abollé, Y. U. Kouakou, O. Kambiré, Y. T. Koné, A. R. Kouakou, Adsorption of Methyl Orange on Corncob Activated Carbon: Kinetic, Equilibrium, and Thermodynamic Studies, Earthline Journal of Chemical Sciences, **2022**, 8(2), 205-224.
14. N. L. B. Kouassi, K. P. D. A. N'goran, L. D. Blonde, D. Diabate, A. Trokourey, Simultaneous Removal of Copper and Lead from Industrial Effluents Using Corn Cob Activated Carbon, Chemistry Africa, **2023**, 6, 733–745.
15. B. Coulibaly, L. A. G. Pohan, O. Kambiré, L. P. S. Kouakou, H. Goure-Doubi, D. Diabaté, L. Ouattara, Valorization of Green Clay from Bouaflé (Ivory Coast) in the Simultaneous Elimination of Organic Pollutants and Metallic Trace Elements by Adsorption: Case of Methylene Blue and Cadmium Ions, Chemical Science International Journal, **2020**, 29(8), 37-51.
16. Y. T. Koné, A. Abollé, O. Kambiré, A. K. Bonito, Use of a Clay from Southern Ivory Coast (Bingerville) for the Adsorption of Methyl Orange in Aqueous Media, American Journal of physical chemistry, **2024**, 13(2), 28-34.
17. K. J. B. Alloko, T. Ekou, L. Ekou, O. Lafon, Adsorption of lead on a natural clay from the agboville region (Côte d'Ivoire) and activated clay with hydrochloric acid. Modeling by linear isotherms of Langmuir and Freundlich, Rasayan J. Chem, **2020**, 13 (3), 1933 - 1943.
18. S. Bendou, M. Amrani, Effect of Hydrochloric Acid on the Structural of Sodic-Bentonite Clay, Journal of Minerals and Materials Characterization and Engineering, **2014**, 2(5), 404-413.
19. N. A. Edama, A. Sulaiman, K. H. K. Hamid, M. N. M. Rodhi, M. Mohibah, S. N. A. Rahim, The Effect of Hydrochloric Acid on the Surface Area, Morphology and Physico-Chemical Properties of Sayong Kaolinite Clay, KEM, **2013**, 594–595, 49–56.
20. H. S. Ndé, P. A. Tamfuh, G. Clet, J. Vieillard, M. T. Mbognou, E. D. Woumfo, Comparison of HCl and H_2SO_4 for the acid activation of a cameroonian smectite soil clay: palm oil discolouration and landfill leachate treatment, Heliyon, **2019**, 5(12), e02926.
21. Y. U. Kouakou, O. Kambire, V. E.-S. Zran, Properties of magnetic carbon base on ricinodendronheudelotii and application in removal of methylene blue. Int. J. Adv. Res., **2022**, 10(11), 440-453.
22. N. L. B. Kouassi, B. H. G. Doubi, D. Diabate, L. D. Blonde, A. Trokourey, Recycling of Alum Sludge for Rhodamine B Removal from Industrial Effluents, Chemistry Africa, **2023**, 6, 485–498.
23. H. Oualid, N. Emmanuel, Modeling of adsorption isotherms of phenol and chlorophenols onto granular activated carbon Part I. Two-parameter models and equations allowing determination of thermodynamic parameters, Journal of Hazardous Materials, **2007**, 147, 381–394.
24. L. P. M.-S. Kouakou, D. Karidioula, M. R. W. Manouan, A. G. L. Pohan, G. Cissé, L. K. Konan, J. Y. Andji-Yapi, Use of two clays from Côte d'Ivoire for the adsorption of methyl red from aqueous medium, Chemical Physics Letters, **2023**, 810: 140183.
25. Y. U. Kouakou, O. Kambiré, K. K. G. Kouakou, A. Trokourey, Study of Potential Adsorption of Glyphosate on Iron-textured Soil, American Journal of Applied Chemistry, **2021**, 9(6), 207-214. doi: 10.11648/j.ajac.20210906.15
26. O. Kambiré, Y. U. Kouakou, A. Kouyaté, S. P. Sadia, K. E. Kouadio, K. J. Kimou, S. Koné, Removal of rhodamine B from aqueous solution by adsorption on corn cobs activated carbon. Mediterranean Journal of Chemistry, **2021**, 11(3), 271-281.

27. L. Wu, X. Liu, G. Lv, R. Zhu, L. Tian, M. Liu, Y. Li, W. Rao, T. Liu, L. Liao, Study on the adsorption properties of methyl orange by natural one-dimensional nano-mineral materials with different structures, Sci Rep, **2021**, 11, 10640.
28. M. B. Desta, Batch Sorption Experiments: Langmuir and Freundlich Isotherm Studies for the Adsorption of Textile Metal Ions onto Teff Straw (Eragrostis tef) Agricultural Waste, Journal of Thermodynamics, **2013**, Article ID 375830.
29. A. Özer, H.B. Pirinççi, The adsorption of Cd(II) ions on sulphuric acid-treated wheat bran, Journal of Hazardous Materials, **2006**, 137(2), 849–855.
30. A. Mittal, A. Malviya, D. Kaur, J. Mittal, L. Kurup, Studies on the adsorption kinetics and isotherms for the removal and recovery of Methyl Orange from wastewaters using waste materials, Journal of Hazardous Materials, **2007**, 148(1–2), 229-240.
31. N. L. B. Kouassi, A. Abollé, A. R. Kouakou, V. Gogbe, A. Trokourey, Using Modified Activated Carbon to Remove Methylene Blue and Rhodamine B from Wastewater, American Journal of Physical Chemistry, **2023**, 12(3): 30-40.
32. B. Abbou, I. Lebkiri, H. Ouaddari, A. E. Amri, F. E. Achibat, L. Kadiri, A. Ouass, A. Lebkiri, E. H. Rifi, Improved removal of methyl orange dye by adsorption using modified clay: Combined experimental study using surface response methodology, Inorganic Chemistry Communications, **2023**, 155, 111127.
33. A. Khenifi, Z. Bouberka, F. Sekrane, M. Kameche, Z. Derriche, Adsorption study of an industrial dye by an organic clay. Adsorption, **2007**, 13, 149–158.
34. E. A. Abo, Y. U. Kouakou, Y. A. Yobouet, A. Trokourey, Adsorption of Remazol Black 5 and Indigo Carmine on Corn Cobs Activated Carbon: Kinetic, Equilibrium, and Thermodynamic Studies, Indian Journal of Advances in Chemical Science, **2021**, 9(2), 69-75. DOI: 10.22607/IJACS.2021.902004
35. M. Kosmulski, pH-dependent surface charging and points of zero charge II. Update, Journal of Colloid and Interface Science, **2004**, 275(1), 214-224.